Self-consistent pseudopotential calculations for Si (111) surfaces: Unreconstructed (1×1) and reconstructed (2×1) model structures*

M. Schlüter,[†] James R. Chelikowsky, Steven G. Louie,[‡] and Marvin L. Cohen

Department of Physics, University of California, Berkeley, California 94720
and Inorganic Materials Research Division, Lawrence Berkeley Laboratory, Berkeley, California 94720
(Received 8 May 1975)

A recently developed method involving self-consistent pseudopotentials has been used to calculate the electronic structure of several Si (111) surface models. The results for (1×1) unreconstructed, relaxed and unrelaxed surfaces are compared with earlier calculations and discussed in terms of density-of-states curves and charge-density distributions. A fully self-consistent calculation has been carried out for Haneman's (2×1) reconstructed surface model. It is found that the important experimental results can be understood using this model, and changes in the electronic structure occurring after reconstruction are rationalized on chemical grounds. In particular infrared-absorption measurements, photoemission measurements, and recent angular-dependent photoemission measurements find consistent explanations.

I. INTRODUCTION

In this paper, self-consistent calculations of the electronic structure of several Si (111) surface models are described. The electronic structure of Si (111) surfaces has been investigated in a large number of experimental studies.[1-9] Most of the experiments have been done on surfaces having either (2×1) or (7×7) superlattice structures which are the metastable and stable surface arrangements of Si(111), respectively. Very useful results, however, have been obtained from theoretical studies on unreconstructed (1×1) surface models.[10-13] In spite of the usefulness of these calculations, only results obtained from realistic reconstructed surface models are consistent with all the experimental data. In the present paper two unreconstructed (1×1) surface models (unrelaxed and relaxed) are investigated before studying (for the first time by a self-consistent method) a realistic (2×1) reconstructed surface model. We note that self-consistency in the present context means the self-consistent electronic response to a given structural model. Even though calculations of this kind can and have been carried out for several structural models [unrelaxed, and (2×1) reconstructed in our case] it is extremely difficult, if not impossible, to compare total energies to determine the most favorable surface structural arrangement. The reasons for this are twofold. First, it is known experimentally that the surface geometry is strongly temperature dependent, therefore free energies involving entropies must be compared. Second, the total surface energies are large quantities which differ only slightly for the different geometries. With the present techniques they cannot be calculated with sufficient precision to yield reliable results for the energy differences. The present calculations as well as all previously existing self-consistent calculations are therefore restricted to the self-con-

sistent determination of the electronic structure in response to a given structural model.

The only other self-consistent approach to the (111) surface of Si has been presented by Appelbaum and Hamann[10] (AH), and like our approach, it is based on the pseudopotential scheme. For metal surfaces, pseudopotential calculations by AH for [14] Na and by Alldredge and Kleinman (AK) for[15] Al and[16] Li have been carried out very successfully. In addition to the specific problems connected with a self-consistent treatment, the main difficulty arises from the absence of periodicity in treating the surface case.

AH solve this problem by expanding the electron wave function in a mixed representation, i.e., two-dimensional plane waves to account for the periodicity parallel to the surface, multiplied by functions that depend on the remaining spatial coordinate z perpendicular to the surface. In this mixed representation, the Schrödinger equation becomes a set of coupled differential equations in the spatial coordinate z which can be integrated stepwise numerically, obeying appropriate boundary conditions between the vacuum and a matching plane somewhere in the cyrstal. Numerical problems and instabilities, however, turn this physically appealing concept into a rather involved procedure.

AK also start with a mixed representation; however, they use a series of analytic trigonometric functions describing the z variation of the wave function perpendicular to the surface. Retaining a finite number of these periodic functions is equivalent to periodically repeating the surface (or better, the thin film). If these films are spaced sufficiently far enough apart from each other, and if they are sufficiently thick, their surfaces can be regarded as noninteracting and representative of the true crystal surface. More precisely, AK expand the z variation of the wave function in a truncated set of trigonometric sine and cosine functions, all

of which individually vanish half-way between the films. We believe that these specific boundary conditions, which are not strictly imposed by the physics of the system, may result in slow convergence behavior since they add an artificial symmetry to the problem.

Our method in contrast to AK's approach uses a set of periodic, trigonometric functions with arbitrary rather than fixed phases.

Using this basis set, our procedure is then completely equivalent to placing the film in a periodic array and expanding the wave function in plane waves in the usual form as for bulk calculations. The most appealing feature of the approach is that the empirical pseudopotential method[17] (EPM) in its simple standard form can now be applied. In particular, *non*-local potentials can easily be incorporated (which is not evident in AH's method), and experience, e.g., about convergence of wave functions, gained in calculations of bulk layer crystals[18] can be used. The method that is adopted for the present study of the electronic structure of Si (111) surfaces, however, goes beyond the standard EPM through the requirement of self-consistency. As reported in earlier papers[13,19] the method may be applied to various kinds of local configurations like atoms, molecules, impurities, vacancies, one-dimensional chains, two-dimensional layers, surfaces, or interfaces. The disadvantages, and also the ultimate limitations, of the method in dealing with complicated systems is connected to the large number of plane waves required to describe the systems' wave functions. The use of symmetry-adapted combinations of plane waves is a helpful tool in dealing with this problem.

The remainder of this paper will be organized as follows. In Sec. II the various steps in the self-consistent calculations are discussed in detail. The results for the electronic structure of unreconstructed, relaxed, and unrelaxed Si (111) surfaces are presented in Sec. III. Section IV contains the discussion of results obtained for a (2×1) reconstructed surface model. In Sec. V the main results are summarized and some concluding remarks are given.

II. CALCULATIONS

In this section a detailed description of the self-consistent calculations is given, carried out on several Si (111) surface models. The method has been described briefly before,[13,19] and was mentioned in Sec. I. The essence of our method of calculation is to retain (artificial) periodicity perpendicular to the surface. In other words, a large elongated unit cell is defined which, in two dimensions, is spanned by the shortest lattice vectors parallel to the surface, i.e., for the unreconstructed surface, hexagonal lattice vectors with the length of $\frac{1}{2}\sqrt{2}a_c$, where $a_c = 5.43$ Å is the lattice constant of bulk Si (the 2×1 reconstructed case will be discussed later), and by a long c axis extending over M atomic layers and N layers of empty space. The numbers M and N have to be chosen such that (a) the film of material is thick enough to effectively decouple the two surfaces on each side of the film and (b) the film surface potential can decay into the "vacuum" without perturbation arising from other periodically displaced films. Various test calculations showed that films of $M = 12$ atomic layers separated by $N \sim 4$ layers of empty space resulting in a lattice constant $c = \frac{5}{2}\sqrt{3}a_c$ fulfill these requirements well for Si. The problem thus consists of self-consistently solving the electronic structure of the "periodic" system whose hexagonal unit cell, with the above-mentioned dimensions, contains 12 Si atoms (for the unreconstructed surface). Proceeding in the standard manner, we expand the electron wave function in plane waves with reciprocal-lattice vectors $\vec{G}$:

$$\psi_{\vec{k}}^n(\vec{r}) = \sum_{\vec{G}} a_{\vec{k}}^n(\vec{G}) e^{i(\vec{k}+\vec{G})\cdot\vec{r}} . \qquad (1)$$

In order to account well for the "structure" in the large unit cell (i.e., the individual atoms or bonds), this expansion has to be carried to sufficiently large $\vec{G}$ vectors. A kinetic-energy cutoff $E_1 = |\vec{G}_{max}|^2 \approx 2.7$ Ry, which is independent of the size of the unit cell, was chosen in accordance with earlier bulk calculations[18] on layer crystals. This cutoff, which corresponds to a cutoff close to $(2, 2, 0)$ in cubic bulk Si, yields about 160–180 plane waves up to $(0, 0, 12)$, which allow sufficient variations of the wave functions inside the unit cell and at the surface. The variations of the calculated total charge inside the film can be compared to bulk charge densities of Si calculated with much larger cutoff energies. Typical differences are of the order of 20% in the peak values of the charge distribution. To improve the energy convergence another 340 plane waves are included via Löwdin's perturbation scheme,[17] which corresponds to a second cutoff at $E_2 = 6.0$ Ry. We would like to mention that the decay of the wave function into the "vacuum" does not represent a particular problem in this context. In fact, the wave functions at the surface decay into the vacuum over about the same length as do wave functions in the bulk of very-covalent crystals (e.g., bulk Si or layer compounds) decay along certain (*no*-bond) directions. This can, e.g., be inferred from the results of AH which, because they are obtained by real space integration at the surface, should be fully converged.

No group-theoretical simplifications were incorporated into the present calculations, since it was desirable to solve Schrödinger's equation for gener-

al $\vec{k}$ points in the two-dimensional (hexagonal) Brillouin zone. The only remaining symmetry operation which would leave these $\vec{k}$ points invariant would be a reflection parallel to the surface plane which, however, is *not* present in the D_{3d} group of the Si (111) films.

The expansion of the wave function leads to a matrix eigenvalue equation of the usual kind:

$$\sum_{\vec{G}'} (H_{\vec{G},\vec{G}'} - E\delta_{\vec{G},\vec{G}'})a_{\vec{k}}(\vec{G}') = 0 , \qquad (2)$$

which is solved by standard methods.[17] The Hamiltonian matrix elements are of the form

$$H_{\vec{G},\vec{G}'} = |\vec{k}+\vec{G}|^2\delta_{\vec{G},\vec{G}'} + V_{PS}(\vec{G},\vec{G}') , \qquad (3)$$

where $V_{PS}(\vec{G},\vec{G}')$ represents a general pseudopotential matrix element.

The present calculations are restricted to the use of *local* pseudopotentials which are known to yield very satisfactory results for bulk Si. The self-consistency loop was entered with an empirical potential

$$V_{emp}(\vec{G}) = S(\vec{G})V_{emp}^{at}(|\vec{G}|) , \qquad (4)$$

where

$$S(\vec{G}) = \frac{1}{M}\sum_{\vec{\tau}_i} e^{-i\vec{G}\cdot\vec{\tau}_i} \qquad (5)$$

is the structure factor describing the atomic positions in the "large" unit cell, and where $V_{emp}^{at}(|\vec{G}|)$ are form-factor values derived from a continuous curve of the form

$$V(q) = \frac{a_1(q^2 - a_2)}{\exp[a_3(q^2 - a_4)] + 1} . \qquad (6)$$

The four parameters a_i in Eq. (6), which are given in Table I, were determined by fitting $V(q)$ to three form-factor values for bulk Si: $V(1,1,1) = -0.2241$ Ry, $V(2,0,0) = 0.0551$ Ry, $V(3,1,1) = 0.0724$ Ry, and renormalizing it for the different unit-cell volume. Some continuous extrapolation of the kind of Eq. (6) is necessary to obtain form factors for the "new" $\vec{G}$ vectors of the surface problem. While the shortest $\vec{G}$ vector in bulk Si(111) has the length of 1.06 a.u., in the surface problem $\vec{G}$ vectors as short as 0.14 a.u. are needed. The empirical potential Eq. (6) is very uncertain at these small $\vec{G}$ vectors, and large changes are expected in the

TABLE I. Parameters entering Eqs. (6) and (13) to define the empirical and ionic Si pseudopotentials.

	V_{emp}^{at}	V_{ion}^{at}
a_1	0.279	-0.992
a_2	2.214	0.791
a_3	0.863	-0.352
a_4	1.535	-0.018

course of self-consistency. The long-range potential fluctuations corresponding to these small $\vec{G}$ vectors are absent in a bulk Si crystal. In the surface case, they are important as they form the surface potential barrier and strongly determine work functions and ionization potentials. The solutions of the eigenvalue problem, Eq. (2), are the energies $E_n(\vec{k})$ and the pseudo wave functions defined by Eq. (1). These quantities were evaluated at 28 $\vec{k}$ points in the irreducible part ($\frac{1}{12}$) of the two-dimensional hexagonal Brillouin zone. This relatively large number of sampling points was chosen, rather than one or several "special" $\vec{k}$ points, to precisely determine the Fermi level and the total valence charge. The *unreconstructed* Si (111) surface is metallic since the Fermi level falls within the "dangling bond" surface band. In this surface band, occupied and unoccupied states differ in their electronic charge distributions, which justifies the "fine" sampling of the Brillouin zone. In the case of "true" semiconducting surfaces, as unreconstructed (110) zinc-blende surfaces or (2×1) reconstructed (111) Si surfaces, we believe calculations based on a few special $\vec{k}$ points will yield good self-consistent results. To determine the Fermi level, the density of states, $D(E)$, was evaluated using the method of Gilat and Dolling,[20] with the necessary energy gradients derived by $\vec{k}\cdot\vec{p}$ techniques. Once the Fermi level E_F was known, the total valence (pseudo) charge density $\rho(\vec{r})$ could be evaluated.

Once the valence charge $\rho(\vec{r})$ is known in terms of its Fourier components $\rho(\vec{G})$, the Hartree-Fock-type screening potentials V_H and V_X can easily be evaluated. V_H is the repulsive Coulomb potential seen by an electron and generated by all the valence electrons. It is defined by Poisson's equation

$$\nabla^2 V_H(\vec{r}) = -4\pi e^2\rho(\vec{r}) , \qquad (7)$$

and it can be written as a Fourier series

$$V_H(\vec{r}) = \sum_{\vec{G}} V_H(\vec{G})e^{i\vec{G}\cdot\vec{r}} , \qquad (8)$$

with

$$V_H(\vec{G}) = 4\pi e^2\rho(\vec{G})/|\vec{G}|^2 .$$

The divergence of $V_H(\vec{G})$ for $|\vec{G}| \to 0$ is physically irrelevant, since it is exactly cancelled by the ionic potential generated by the positive Si^{+4} ion cores (over-all charge neutrality). We can therefore arbitrarily set $V_H(\vec{G}=0) = V_{ion}(\vec{G}=0) = 0$. Numerically, however, the divergent character of $V_H(\vec{G})$ [and $V_{ion}(\vec{G})$] for small $\vec{G}$ values poses stability problems, as we shall discuss later. The nonlocal Hartree-Fock exchange potential $V_X(\vec{r},\vec{r}')$, which if added to the Hartree potential $V_H(\vec{r})$ cancels the electron self-energy contained in $V_H(\vec{r})$, has been approxi-

mated using the statistical exchange model of Slater.[21] Only the valence charge is included in calculating V_x. Core-valence cross terms are localized in the core region and are believed to have little effect on the self-consistent valence electron structure of Si. It thus has the local form

$$V_x(\vec{r}) = -\alpha 3e^2 (3/8\pi)^{1/3} [\rho(\vec{r})]^{1/3} . \qquad (9)$$

In the present calculations the value $\alpha = 0.79$ is used in accordance with AH, which brings Slater's exchange in agreement with Wigner's[22] interpolation formula at the average valence charge density of Si. In addition, bulk calculations with $\alpha = 0.79$ have yielded satisfactory results. The function $[\rho(\vec{r})]^{1/3}$ has been obtained by evaluating

$$\rho(\vec{r}) = \sum_G \rho(\vec{G}) e^{i\vec{G}\cdot\vec{r}}$$

at a three-dimensional grid of $N \sim 10\,000$ $\vec{r}$ points sampling the real space unit cell. The cube root has then been taken at each individual $\vec{r}$ point, and the resulting function $[\rho(\vec{r})]^{1/3}$ has been transformed back into Fourier space according to

$$\rho^{1/3}(\vec{G}) = \frac{1}{N} \sum_{\vec{r}_i} [\rho(\vec{r}_i)]^{1/3} e^{-i\vec{G}\cdot\vec{r}_i} . \qquad (10)$$

The precision of this procedure can easily be tested by omitting the step at which the cube root of $\rho(\vec{r}_i)$ is taken. The final $\rho(\vec{G})$ should then be identical to the initial values. The exchange potential then has the form

$$V_x(\vec{r}) = -\alpha (3/2\pi) e^2 (3\pi^2)^{1/3}$$

$$\times \sum_G \rho^{1/3}(\vec{G}) e^{i\vec{G}\cdot\vec{r}} . \qquad (11)$$

The exchange potential is an absolute potential which approaches zero in the vacuum as the charge goes to zero. $\rho^{1/3}(\vec{G}=0)$ has a finite value and is essential in determining the absolute value of the potential. The sum of the two potentials $V_H(\vec{r})$ and $V_x(\vec{r})$ yields the electronic screening potential

$$V_{\text{screen}}(\vec{r}) = \sum_G [V_H(\vec{G}) + V_x(\vec{G})] e^{i\vec{G}\cdot\vec{r}} \qquad (12)$$

and is at each step in the self-consistent loop evaluated from the total valence charge.

After initiating the calculations with an empirical potential V_{emp} [Eq. (4)], the self-consistent loop is continued by adding the screening potential V_{screen} to an ionic potential V_{ion} generated by the Si^{+4} ionic cores. This ion pseudopotential contains, in addition to the exchange α, the only parameters of the self-consistent calculation. First, there are the atomic positions in the surface which enter V_{ion} via a structure factor given by Eq. (5). In addition to the structure model, the individual atomic ionic potential is also based on a parametrized

model. Assuming that, to first order, the ion cores do not change in the free ion, in the bulk crystal, or in the surface, an atomic model potential which was fitted to atomic-term values (as done by Heine and Abarenkov[23]) has been used in our calculation. One important (but not sufficient) check on the quality of this potential is to use it to perform a self-consistent Si bulk calculation. This test is not sufficient, since bulk calculations do not probe the long-range Coulomb tail of ionic potentials. In the case of surfaces, however, this tail is of importance. On the other hand, the Coulomb tail is model independent and results in a $1/q^2$ behavior of the Fourier-transformed potential for small wave vectors.

The repulsive cores of the ionic model potentials fitted by Heine and Abarenkov to atomic term values are nonlocal of l dependent. In the present calculation, a local, "on Fermi sphere" approximation was used in deriving the Fourier transform. This Fourier transform was fitted to a four-parameter curve of the form

$$V_{\text{ion}}^{\text{at}}(q) = (a_1/q^2)[\cos(a_2 q) + a_3] e^{a_4 q^4} . \qquad (13)$$

The values of these four parameters are given in Table I. The potentials are normalized to an atomic volume of 169 in atomic units (a. u.), and the units are Ry if q is entered in a. u. Equation (13) behaves like $1/q^2$ for small q, representing the Coulomb tail, and decreases exponentially for large q, allowing a definition of a reasonable cutoff $q_c \approx 3$ a. u. for Si^{+4}. As mentioned above, self-consistent Si bulk calculations based on this ionic pseudopotential, yield a band structure that is in excellent agreement with the most recent empirical calculations.[24] The most important electronic transition energies are reproduced to within ± 0.1 eV. The total bulk valence charge derived from this self-consistent bulk calculation compares very favorably with the empirical charge densities of Walter and Cohen.[25] The values of charge densities in the bonds change from 25.5 to 25.8 electrons per unit cell, and at the atomic sites from 7 to 5.5, which results from a more repulsive self-consistent potential at the atoms.

The input potentials for steps $n = 1$ and 2 of the self-consistent loop then become

$$V_{\text{in}}^{(1)}(\vec{r}) = V_{\text{emp}}(\vec{r}) ,$$

$$V_{\text{in}}^{(2)}(\vec{r}) = V_{\text{ion}}(\vec{r}) + V_{\text{screen}}^{(1)}(\vec{r}) . \qquad (14)$$

Note that, while $V_{\text{emp}}(\vec{r})$ and $V_{\text{ion}}(\vec{r})$ are linear superpositions of atomic potentials, all other potentials $V_{\text{screen}}^{(n)}$ and $V_{\text{in}}^{(n+1)}$ ($n \geq 1$) are of a more general form and can no longer be factorized into structure factor times form factor. This fact accounts for the nonlinear nature of the dielectric screening and results in the existence of "forbidden" reflections
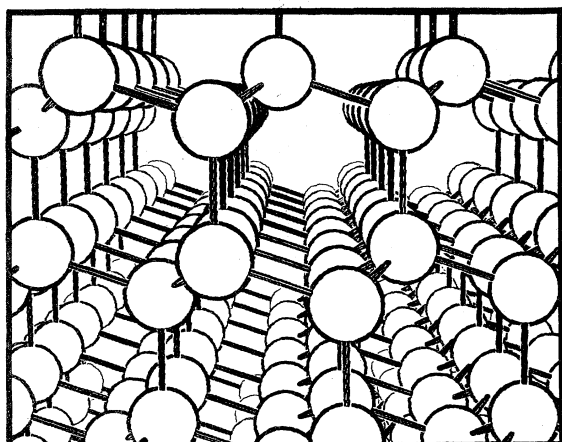
FIG. 1. Perspective view of the Si crystal structure projected on a (110) plane. [111] direction is vertical. (111) surface is obtained by cutting the vertical bonds in a horizontal plane.

in the self-consistent potential.

Since the potential $V_{emp}(\vec{r})$ was determined empirically for Si bulk crystals, it is not expected to yield a very good screening charge for a surface described by the ionic cores $V_{ion}(\vec{r})$. In fact, $V_{in}^{(2)}(\vec{r})$ results in a very different eigenvalue spectrum and charge than does $V_{in}^{(1)}(\vec{r})$, and any further steps in the self-consistent loop based on a straightforward extension of Eq. (14) would be unreasonable and would not converge. This very unstable behavior of the self-consistent potentials in particular, for the small $\vec{G}$ vectors, has already been described by Lang and Kohn[26] and by AK.[16] In agreement with these authors we also find that relaxed, modified versions of Eqs. (14) which compute the input potential of stage $(n+1)$ from a linear mixture of input and output potentials of stage (n) does not result in a convenient method to attain rapid convergence for the surface problem. In the present calculations, these instabilities were dealt with by computing adjusted input potentials $V_{in}^{(n)}(\vec{G})$ for $n > 2$ from preceding input and output potentials individually for each small $\vec{G}$ vector. This can best be done by inspecting V_{out} vs V_{in} separately for each small $\vec{G}$ and by interpolating graphically between the calculated values. Even though the various Fourier components are *not* independent, this procedure helps to reach convergence fairly rapidly. Mathematically, the instabilities are reflected in rather steep curves (with negative slopes) of V_{out} vs V_{in}, i.e., very small changes in V_{in} result in large overshoots in V_{out}. For higher $\vec{G}$ vectors, $|\vec{G}| \geq 1$ a.u., no instabilities occur and convergence is easily reached. Because of the above-mentioned instabilities and difficulties in determining long-range potential fluctuations, work functions and

ionization potentials are difficult to obtain correctly by our method.

III. RESULTS FOR UNRECONSTRUCTED Si (111) SURFACES

Clean unreconstructed Si (111) surfaces are known to be thermodynamically unstable below 900 °C.[1] Stability can be reached at lower temperatures by adsorption of adatoms.[7] Nevertheless, the clean unreconstructed surface presents an excellent model for the theoretical study of surface effects,[10-12] and results obtained for it can be compared to subsequent more elaborate (reconstructed) surface calculations. Our study of the Si (111) surface therefore starts with the clean, unrelaxed, unreconstructed surface, in which all surface atoms remain at their exact "bulk" positions. In a second ("relaxed") model the outermost atomic layer was rigidly relaxed inwards by an amount of $\Delta = 0.33$ Å as proposed by AH.[10] In Fig. 1, the crystal structure of Si is viewed in perspective along with the [110] direction. The [111] direction is vertical. A horizontal (111) surface is obtained by cutting all vertical bonds in a plane.

An excellent over-all impression of the behavior of the electronic states at the Si (111) surface can be obtained by considering the total, self-consistent valence charge distribution, as presented in Fig. 2, for the unrelaxed surface model. The figure shows charge density contours in a (110) plane cutting the (111) surface at right angles (see Fig. 1). The plotting area starts midway between two films and extends about $4\frac{1}{2}$ atomic layers into the bulk. The atomic (unrelaxed) positions are indicated by dots. Moving deeper into the crystal, the charge distribution closely resembles the Si bulk charge densities; near the surface, it decays rapidly into the "vacuum." This rapid decay assures the required "vacuum" and hence the decoupling of the films. No surface states can be recognized on this plot, since only a small number of them exists in a continuum of decaying bulklike states. It is instructive to compare the charge distribution deeper inside the crystal to the standard, highly convergent Si bulk charge densities of Walter and Cohen.[25] These bulk charge densities which were derived from wave functions including about 90 plane waves up to $\vec{G} = (3, 3, 1)2\pi/a_c$ have values of 25.5, 7, and 11 electrons per bulk unit-cell volume $\Omega = \frac{1}{4}a_c^3$ for the bonding site, the atomic site, and the antibonding site, respectively. Owing to the lower degree of convergence in the present surface calculations, the charge density reaches values of 20, 9, and 12 at the respective sites. This lack of charge "modulations," which amounts to about 25% at the bonding sites, results in an error in the exchange potential ($\sim \rho^{1/3}$) of at most 8% at the bonding sites. We believe that this range of uncertainty in the potential or charge is acceptable
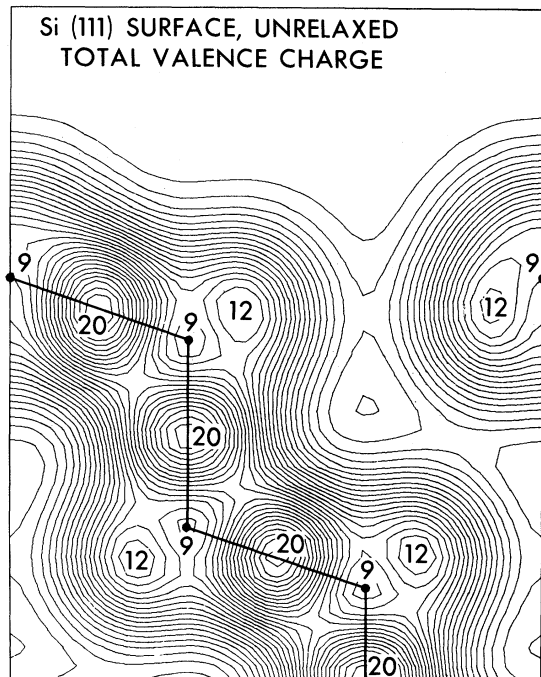
FIG. 2. Total valence charge distribution for an unrelaxed Si (111) surface. Charge is plotted as contours in a (110) plane intersecting the (111) surface at right angles. Plotting area starts in the vacuum and extends about $4\frac{1}{2}$ atomic layers into the crystal. Atomic positions and bond directions are indicated by dots and heavy lines, respectively. Contours are normalized to electrons per Si bulk unit-cell volume $\Omega_0 = \frac{1}{4}a_c^3$.

ic site, and -1.6 (-1.0) at the antibonding site, respectively. The self-consistent potential at the bonding sites differs slightly for the different bonds, thus causing some asymmetries in the bond charge distributions. Note the more repulsive core of the self-consistent potential resulting from the model ion potential used. As mentioned earlier, both potentials lead to very similar bulk energy spectra and bulk charge densities. The self-consistent potential of AH for a relaxed surface model reaches values around -2.2, >0.2, and -1.6 at the bonding

and does not influence the results more than other conceptual uncertainties, like the choice of the factor α scaling Slater's exchange potential. The total charge density can also be compared with results obtained by AH for a relaxed Si (111) surface.[10] (The outermost atomic layer has been relaxed inwards by 0.33 Å.) Scaling their charge contour plot by the volume Ω, the values 20, 3, and 10 (± 2) are obtained for the respective sites. Their particularly low value at the atomic site might result from a stronger repulsive core potential.

In Fig. 3, contour plots are presented of the self-consistent pseudopotential giving rise to the valence charge discussed above and of the empirical starting potential. The potentials are displayed in the same plane as the charge in Fig. 2, with values given in rydbergs. Self-consistency was reached after 5–7 steps within 0.01 Ry, except for the long-wavelength components of the potential which merely determine the vacuum level and the ionization potential. Normalized to approach zero in the vacuum, the potential values for the self-consistent and empirical potentials are -1.8 (-1.8) at the bonding site, $+0.8$ ($+0.1$) at the atom-
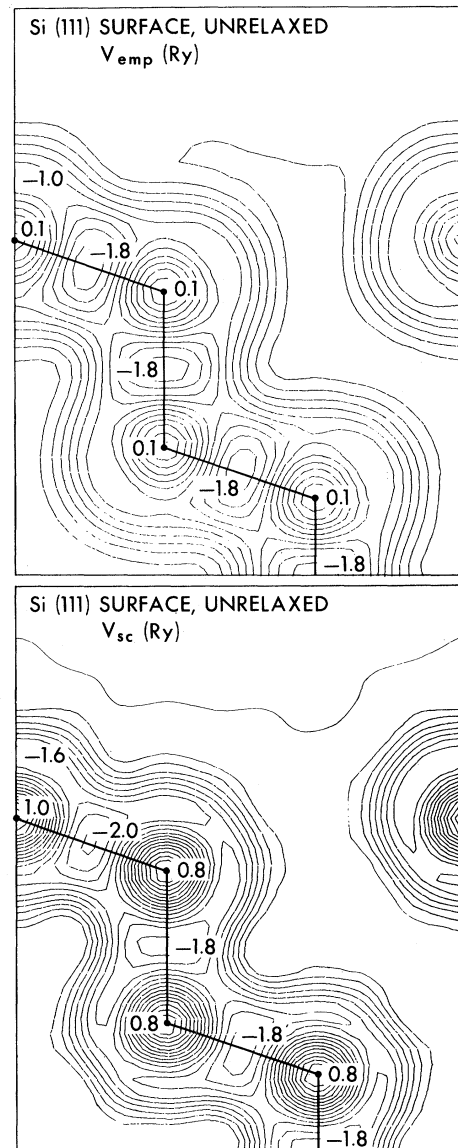

FIG. 3. Contour plots of the empirical starting potential V_{emp} (top) and the final self-consistent potential V_{sc} (bottom). Plotting areas are identical to Fig. 2. Potential values are given in rydbergs normalized to zero in the vacuum.
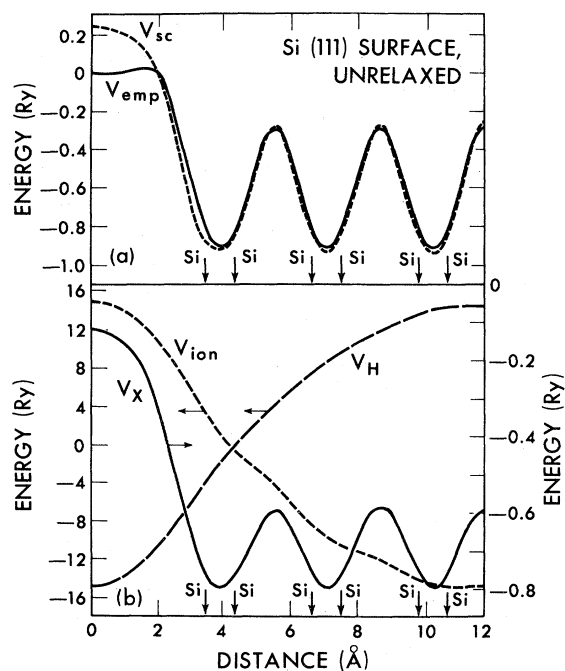
FIG. 4. (a) Empirical (V_{emp}) and self-consistent (V_{sc}) potentials averaged parallel to the (111) surface, plotted as a function of the coordinate z perpendicular to the surface. (b) Individual potential contributions adding up to the self-consistent potential V_{sc} of Fig. 4(a).

site, atomic site, and antibonding site, respectively. This is in good agreement with our self-consistent potential except possibly at the atomic site where the AH value is not explicitly given in Ref. 10.

To illustrate the various contributions to the total self-consistent potential in Fig. 4(b), the potentials $V_{ion}(z)$, $V_H(z)$, and $V_X(z)$ averaged parallel to the surface are plotted as a function of the coordinate z perpendicular to the surface. Owing to their strong long-range Coulomb character, V_{ion} and V_H show only small short-range fluctuations compared to their absolute values. V_{ion} rises about 30 Ry over the last six atomic layers and forms a strong surface barrier. It is very delicately balanced by the screening potential V_H leaving a weak attractive net potential with fluctuations on the scale of interatomic distances of the order of 0.5 Ry. Strictly speaking, only the sum of V_H and V_{ion} is physically meaningful; the individual potentials diverge as $|\vec{G}|_{min}^{-2}$.

The sum is added to the exchange potential V_X, which is of comparable strength and modulation. The resulting total self-consistent potential is indicated in Fig. 4(a). In this figure, the original empirical starting potential is superimposed to demonstrate the change in the potential that occurs because of the self-consistency procedure. While

inside the crystal the two potentials $V_{emp}(z)$ and $V_{sc}(z)$ are almost identical (the potential differences visible in Fig. 3 cancel almost exactly after averaging parallel to the surface), the self-consistent potential $V_{sc}(z)$ is somewhat deeper at the outermost atomic layer and exhibits a higher surface barrier of about 0.2 Ry. These changes localize the charge more in the surface, stabilize the surface states, and increase the ionization potential. In fact, using the empirical starting potential, charge originating from states at the top of the valence bands was leaking out into the "vacuum." This charge was confined back to the surface by the stronger potential obtained in course of self-consistency. Though the differences between the empirical and self-consistent surface potentials seem to be relatively small, they are essential to stabilize the surface. An ionization potential of about 4.0 eV has been calculated. As mentioned earlier, this quantity is difficult to determine precisely with our method and the calculated value is only approximate (± 1 eV).

Figure 5 displays the two-dimensional band structure of a twelve-layer Si (111) film based on the self-consistent potential for the relaxed surface model. The band structure is presented for surface $\vec{k}$ vectors, $\vec{k}_{||}$, between $\Gamma(0, 0)$, $M(\frac{1}{2}, 0)$, $K(\frac{1}{3}, \frac{1}{3})$ and $\Gamma(0, 0)$. The 24 valence bands can be roughly divided into three bulk groups, representing the six low-lying s-like bands, six bands of mixed s and p character, 11 p-like bands, and one separate p-like dangling-bond band in the fundamental gap. The three groups of bands would, with increasing film thickness, approach continua separated by several gaps in which most of the surface states appear.
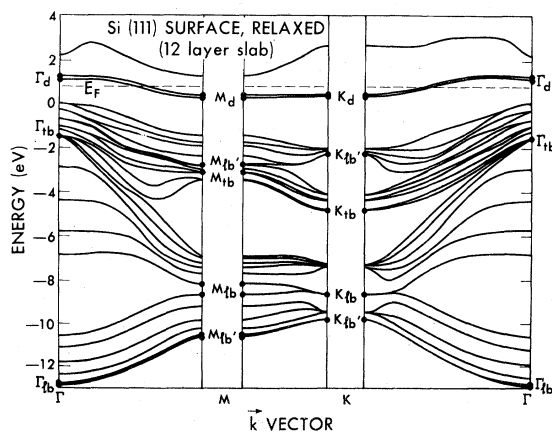

FIG. 5. Two-dimensional band structure of a 12-layer Si(111) film (relaxed surface model). The energy is plotted as a function of $k_{||}$ in the two-dimensional hexagonal Brillouin zone. Various surface states or strong surface resonances at high-symmetry points are indicated by dots and labeled according to the description in the text.

Let us first discuss the dangling-bond bands in the fundamental gap. Suppose a Si bulk crystal is cut even 12 layers, parallel to the (111) plane, and the pieces are gradually separated from each other. With increasing distance, one state each would split away from both the valence bands and the conduction bands to meet about at half-gap to form the twofold-degenerate dangling-bond surface band corresponding to the broken bonds on either side of the Si films. In Fig. 5, the two bands are not exactly degenerate, corresponding to some weak interaction (~ 0.2 eV) still present between opposite surfaces of the 12-layer films. If the surfaces are unrelaxed and unreconstructed, the two dangling-bond bands show almost no dispersion parallel to the surface, i.e., they would appear extremely flat in the band-structure plot. If the outermost atomic layer is relaxed inward, the dangling-bond band shows an increased dispersion parallel to the surface together with a slight over-all shift of the bands (see Fig. 5). This effect shall be discussed later in more detail in relation to charge densities and densities of states. In contrast to the dangling-bond surface band which exists throughout the two-dimensional Brillouin zone independent of relaxation, other surface states show up only in parts of the two-dimensional Brillouin zone, and some depend on relaxation. They are indicated by dots in Fig. 5 at the high-symmetry points Γ, K, and M. A region of particular interest is around the point K. Strongly localized surface states exist in the gap between -7 and -9 eV, independent of surface relaxation. These states merge into the continuum at M and become strong surface resonances. A similar behavior is found around K between -2 and -4 eV. Even though the existence of these surface states does not depend upon relaxation, their exact energy position is a function of relaxation. Other surface states appear only after relaxation, like the splitting away of the lowest valence-band pair between -9.5 and -12.5 eV throughout the zone. All these findings have qualitatively also been obtained in a recent analytical model calculation by Falicov and Yndurain.[27]

Comparison with a tight-binding surface band structure calculated by Pandey and Phillips[12] (PP) shows qualitative agreement, though quantitative differences exist in energy and number of surface states. In particular, five surface states are found in our calculations at K which agrees with the calculations of Falicov and Yndurain, whereas PP only report four surface states. The existence of more than four surface states at a given vector $\vec{k}_{\parallel}$ indicates that bonds deeper in the crystal, not connected to the outermost layer, are strongly affected by the surface. The character of the various surface states will be discussed later in terms of charge density distributions.
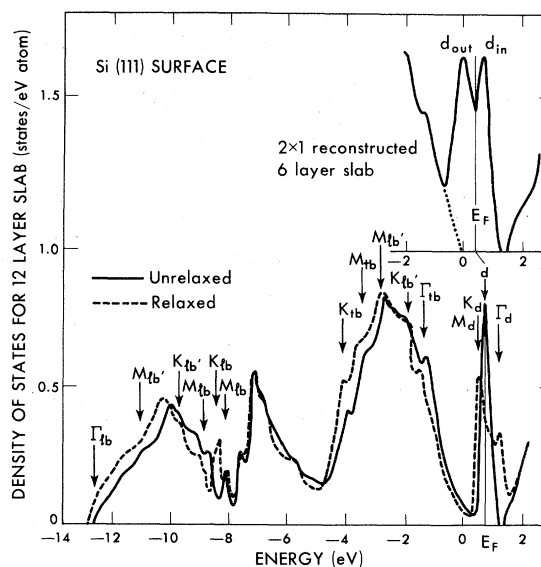

FIG. 6. Density-of-states curves for the self-consistent results on 12-layer films for the relaxed (broken line) and unrelaxed (solid line) surface geometry. Surface states are indicated by arrows and labeled according to Fig. 5. Inserted is the density of states in the vicinity of the fundamental gap for a 6-layer (2×1) reconstructed surface model.

Density-of-states curves for the self-consistent results for the unrelaxed and relaxed surface model are presented in Fig. 6. Since these curves represent the total density of states for a 12-layer slab, their over-all features strongly resemble those of the Si bulk density of states. The results for the (2×1) reconstructed surface (insert) are obtained for a 6-layer slab. They shall be discussed in Sec. IV together with 12-layer (2×1) reconstructed surface calculations. To locate structures associated with surface states (no distinction is made in the present case between bona fide surface states and strong surface resonances), we investigated the charge-density distributions for small energy intervals scanning the entire width of the valence bands. One problem which arises, when stimulating surfaces by finite slabs of atoms periodically repeated, is spurious structure in the density of states due to the "unreal" periodicity of isolated slabs perpendicular to the surfaces. Spurious two-dimensional singularities occur. Their number increases with the number of atomic layers per slab. For the "true" surface case these singularities become "dense" and disappear. For finite-slab calculations, all structures in the density of states have to be investigated in this spirit. Similar problems are encountered when simulating an amorphous material by large unit cells periodically repeated.[28] The locations of surface states and strong surface resonances (for the *relaxed* case)

TABLE II. Calculated energies of surface states and strong surface resonances of the relaxed Si (111) surface at Γ (center), K (corner), and M (edge midpoint) of the two-dimensional Brillouin zone. Also indicated are experimental ultraviolet photoemission spectroscopy (UPS) results for (2×1) and (7×7) reconstructed surfaces. The energy zero is taken at the bulk valence-band edge E_V.

	SCLC[g]		AH[e]	PP[f]	Experiment (2×1)	(7×7)
			(1×1) Relaxed surface			
Γ	1.2	Γ_d	0.88	1.04		
	−1.5(2×)	Γ_{tb}	−1.95(2×)	−1.71(2×)	~−1.0[d]	−1.5[a]
	−12.7	Γ_{lb}	−12.87	−12.9	−11.7[a]	−12.3[a]
					−0.5[a]	
K	0.5	K_d		0.11	−0.45[b]	0.1[a]
					−0.6[c]	
	−2.0	$K_{lb'}$				
	−4.2	K_{tb}		−5.65		
	−8.5	K_{lb}		−8.35		−7.5[a]
	−9.8	$K_{lb'}$		−9.6		
M	0.5	M_d	0.04	0.17		
	−2.6	$M_{lb'}$				
	−3.1	M_{tb}	−3.55	−3.78		−3.6[a]
	−8.1 / −8.7	M_{lb}				
	−10.7	$M_{lb'}$				

[a]Reference 6.   [d]Reference 9.   [f]Reference 12.
[b]Reference 2.   [e]Reference 10.   [g]This work.
[c]Reference 3.

are indicated by arrows in Fig. 6. Their labeling corresponds to the regions around high-symmetry $\bar{k}$ points in the two-dimensional Brillouin zone from which they originate (see dots and labeling in Fig. 5). The surface state energies are given in Table II and compared to experimental data obtained from ultraviolet photoemission spectroscopy (UPS) measurements on (2×1) and (7×7) reconstructed surfaces. Also indicated in Table II are the results of the self-consistent pseudopotential calculation of AH and of the empirical tight-binding calculation of PP on unreconstructed relaxed Si(111) surfaces.

Let us now examine the various surface bands in more detail. When relaxing the outermost atomic layer rigidly inwards by an amount of $\Delta = 0.33$ Å, a surface band (twofold quasidegenerate in our model originating from the two surfaces of the slab) throughout the entire zone splits off between −11 and −13 eV. It essentially corresponds to s-like states with some p_z admixture (centered on the two outermost atomic layers) which decay into the crystal. A typical charge-density plot of these surface states near Γ (Γ_{lb}) at about −12.7 eV is shown in Fig. 7 (top). As one follows this surface band from Γ to M to K the charge center moves somewhat back into the crystal, e.g., the charge distribution of the state $K_{lb'}$ at about −9.8 eV is mostly s-like on the *second* atomic layer with charge extending considerably into the "longitudin-

al" bond between second and third atomic layer. A similar situation is found at M for the state $M_{lb'}$ at about −10.7 eV. At these two points (K and M) the predominant s-like charge on the outermost layer is transferred to the surface states K_{lb} and M_{lb} at somewhat higher energies around −8.5 eV. These states (in particular, K_{lb}) are strongly localized on the outermost layer [see Fig. 8 (bottom)] and decay into the crystal being localized at every other layer (1, 3, 5, etc.). Roughly, it can therefore be said that at K the state $K_{lb'}$ at −9.8 eV has s-like charge on the second, fourth, etc., atomic layer, decaying into the bulk, whereas the state K_{lb} at −8.5 eV has decaying s-like charge at the first, third, etc., atomic layer.

The next surface states of strong surface resonances appear only at considerably higher energy, and they correspond to mostly p-like states with some s admixture. Starting at Γ at −1.5 eV (Γ_{tb}), a twofold-degenerate (fourfold in our case of two surfaces) surface band appears corresponding to the transverse back bonds between first and second atomic layer; its charge distribution is shown in Fig. 7 (bottom). This band merges into the continuum as one goes from Γ to M, where it appears as a strong resonance. Again a region of special interest is at K. A very similar arrangement to the low-lying s states is found for the energies of the p states. The bulklike states merge into two narrow groups of bands separated by a ~2-eV gap
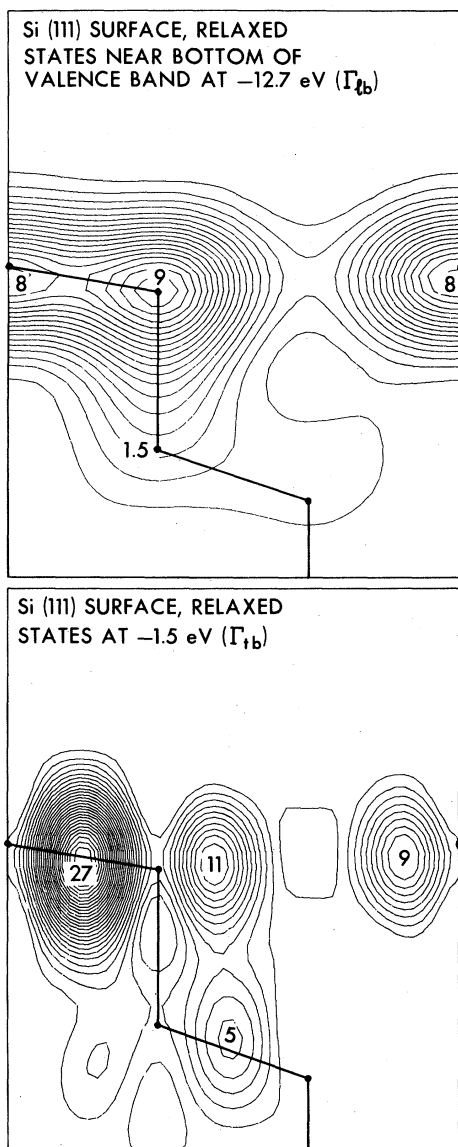
Si (111) SURFACE, RELAXED
STATES NEAR BOTTOM OF
VALENCE BAND AT −12.7 eV (Γ_{lb})

Si (111) SURFACE, RELAXED
STATES AT −1.5 eV (Γ_{tb})

FIG. 7. Charge-density contour plots for two surface states at Γ. States (Γ_{lb}) at −12.7 eV form the bottom of the valence bands (top figure), the transverse back bonds Γ_{tb} (bottom figure), are located −1.5 eV below the valence-band maximum. Indicated charge values are only for comparison.

p states at K. This kind of dehybridization decreases band dispersion, localizes states, and favors the formation of the surface states. In fact, it is the special form of the structure factor at K which allows separation into s states centered on even- or odd-numbered layers, longitudinal p states, and transverse p states.[27] To support this statement further we note that the charge distribution for the state K_{tb} at −4.2 eV is almost identical to the charge of the states Γ_{tb} at −1.5 eV, [see Fig. 7 (bottom)] and therefore has strong transverse character appearing between the first and

Si (111) SURFACE, RELAXED
STATES AT −2 eV (K_{tb}')

Si (111) SURFACE, RELAXED
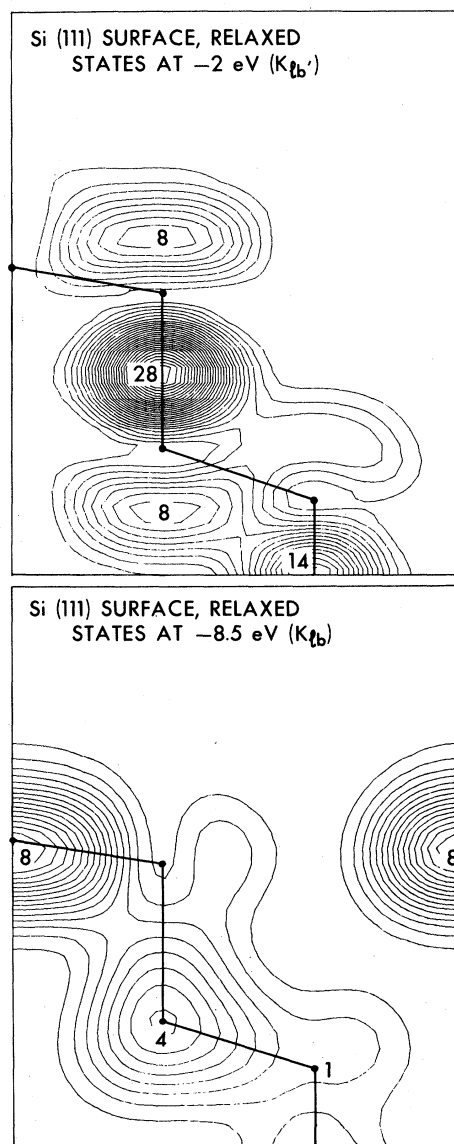STATES AT −8.5 eV (K_{lb})

FIG. 8. Charge-density contour plots for two surface states at K. Longitudinal p-like back-bond orbitals K_{lb}' (top figure) are located at −2 eV, while the s-like charge K_{lb} localized on the outermost, third, etc., atomic layers (bottom figure) has an energy of −8.5 eV.

(see Fig. 5). One surface state (K_{lb}') is found inside this gap at about −2 eV. In contrast to the s-like surface state K_{lb} at −8.5 eV, this state does not appear midgap; a small potential perturbation might have moved this more sensitive p-like state slightly up, towards the upper group of bulklike bands. Another surface state (K_{tb}) splits off below the lower group of bulklike bands at −4.2 eV. The resemblance between the s- and p-like band structure at K, and an inspection of the corresponding charge densities, suggest very strong decoupling of s and

second, third and fourth, etc., layer. The state $K_{tb'}$ at -2.0 eV [see Fig. 8 (top)] is of longitudinal character, the charge appears in the longitudinal bonds between the second and third, fourth and fifth, etc., layer, decaying into the crystal. We would like to note that the behavior of surface states being localized at alternating atomic layers is not an artifact connected with the finite-slab approximation; it has analytically been confirmed for semi-infinite surface models.[27]

In contrast to Γ where two transverse back bond states exist, at K only one such surface state appears, the other having merged into the continuum. Again the situation at M is similar to that at K, with smaller gaps, however, and surface states merging into the continuum. The preceding analysis showed clearly that surface states can "penetrate" deeply into the longitudinal bond between second and third layer, which puts severe restrictions on the size of model clusters representing the surface, and which has to be considered in positioning a matching plane as used by AH separating the surface region from the bulk. It can be inferred from Fig. 6 that inward relaxation strengthens the transverse back bonds and therefore lowers the energies of the states Γ_{tb} and K_{tb}. It weakens the longitudinal back bonds and raises the energy of states like $K_{tb'}$. These effects are also reflected in the total charge density. They shall be discussed again in connection with the (2×1) reconstructed surface.

The most prominent surface states are the dangling-bond states in the fundamental gap. In both the unrelaxed and relaxed cases, the surface bands are half occupied leaving the surface metallic with a Fermi level positioned as indicated in Figs. 5 and 6. A charge-density plot for the occupied part of this band is presented in Fig. 9. The charge originates from states around M and K and exhibits the very pronounced dangling-bond character. The unoccupied states originate from a region around Γ and show some stronger mixing with back bond states. Though the comparative study of the unrelaxed and relaxed surface yields very useful information about the existence energy positions and energy shifts of surface states, these two surface models cannot satisfactorily explain a number of experiments. These experiments include various photoemission measurements,[29] surface mobility studies,[1] and photoconductivity[1] and infrared-absorption measurements[4] on freshly cleaved Si (111) surfaces, exhibiting a (2×1) reconstruction. The most important experimental facts which cannot be explained involve the surface states in and close to the fundamental gap. To gain some understanding of the behavior of these states after (2×1) reconstruction, and to find explanations for the various experimental results, we have done fully self-consistent calculations on a (2×1) reconstructed surface model.

A detailed discussion of this surface model and the results obtained is given in Sec. IV.

IV. RESULTS FOR (2 × 1) RECONSTRUCTED Si (111) SURFACE MODEL

Carefully cleaved clean Si (111) surfaces exhibit a (2×1) superstructure, as seen from low-energy-electron diffraction (LEED) patterns. At the present time, unfortunately, there does not exist a satisfactory analysis of the LEED intensities which would uniquely determine the (2×1) surface geometry. Any calculation of the electronic structure of the (2×1) surface is therefore necessarily based on empirical structural models. The situation is complicated by the fact that the (2×1) reconstructed surface is metastable. It transforms into a more complex (7×7) structure upon annealing, which is the thermodynamically stable Si (111) surface geometry, or it transforms into the simple (1×1) structure after adsorption of adatoms. Once annealed or contaminated the (2×1) structure cannot be recovered. Because of this fact, models for the metastable (2×1) surface cannot easily be established on thermodynamical grounds. Various different reconstruction models have thus been suggested.[8] Most recent discussions seem to favor the formation of the (2×1) superstructure by periodically raising and lowering rows of surface atoms leaving a buckled surface. This model for reconstructed surfaces was first suggested in 1961 by
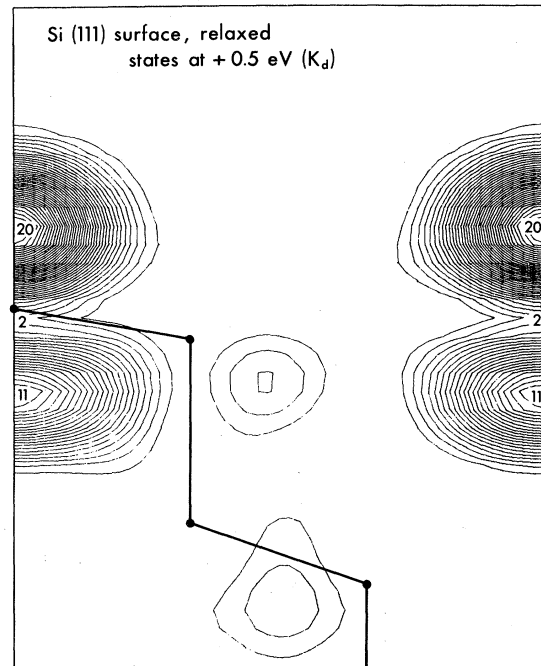

FIG. 9.   Charge-density contour plot of the dangling-bond state K_d at 0.5 eV around the points M and K in the Brillouin zone.
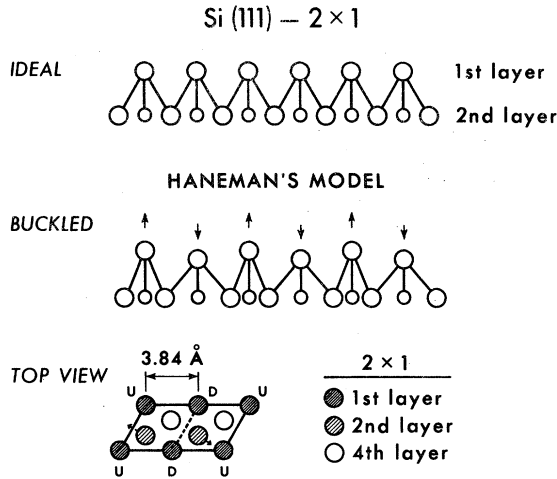
FIG. 10. Schematic representation of the ideal and (2×1) reconstructed Si (111) surface. Reconstruction is done according to Haneman's model (Ref. 29) and leaves the surface buckled as indicated by arrows. Slight lateral shifts of second-layer atoms are also indicated by arrows.

Haneman[29] and later developed by Taloni and Haneman.[30] In addition to the periodic raising and lowering of rows of surface atoms, in Haneman's model, the second-layer atoms are slightly shifted laterally to approximately conserve the individual bond lengths of the transverse back bonds between first and second layer. The situation is schematically indicated in Fig. 10. Without the lateral shift of second-layer atoms transverse back bonds of different lengths would exist. This modified Haneman model has recently been proposed by AH.[31] In their model calculations done on two differently relaxed (inward and outward) (1×1) surfaces, the main emphasis has been put on the existence of stretched and compressed back bonds. The subsequent discussion of our results obtained for a (2×1) Haneman model, however, will show that all essential experimental findings can be understood even if the lengths of the transverse back bonds are approximately conserved.

The structural parameters entering our (2×1) reconstructed surface model are the following: alternating rows of atoms have been raised by 0.18 Å and lowered by 0.11 Å, and second-layer atoms have been shifted laterally, as indicated by the arrows in Fig. 10, such as to approximately preserve the length of the back bonds. This choice of parameters may not represent an optimum choice. In particular, since these parameters represent an overall *outward* relaxation of the outermost atomic layer, some surface states which depend on inward relaxation like the states Γ_{1b} at the bottom of the valence bands will become delocalized. Our main interest in this study, however, is the behavior of the electronic state. in the vicinity of the gap and their dependence on the *character* of the reconstruction (buckling with preserving the length of back bonds). The planar unit cell now contains four atoms. First, preliminary calculations have been done on six-layer slabs separated by three bond lengths of empty space. The corresponding density of states in the vicinity of the valence band edge, obtained from 72 $\vec{k}$ points in the two-dimensional Brillouin zone, is shown as an insert in Fig. 6. As expected, qualitative changes compared to the unreconstructed (1×1) case occur. Doubling the real space unit cell in one dimension corresponds to folding back the Brillouin zone in certain directions. Thus *two* surface bands appear, separated by a gap resulting from the potential perturbation of the reconstruction. This behavior is reflected by the density of states in Fig. 6 showing two peaks which now correspond to two different bands. In Fig. 6, the density of states does not vanish between the two peaks, thus leaving the surface semimetallic. In fact, the gap between the two surface bands is comparable or smaller than their dispersion. We believe that this behavior is an artifact of only including six layers per slab. The surface states on opposite surfaces of the slab show too much interaction, consequently causing the semimetallic behavior.

To obtain more quantitative results (2×1) calculations with 12 layers per slab have been performed. Because of the large matrix size (about 320 plane waves were included to obtain the same convergence as for the unreconstructed cases), the self-consistent calculations were based on a two-point scheme $[(0,0)\Gamma$ and $(\frac{1}{2},\frac{1}{2})K']$. For the final self-consistent potential, several $\vec{k}_{\parallel}$ points along high-symmetry directions have also been included. A band structure showing the bands in the vicinity of the fundamental gap is presented in Fig. 11. The two dangling-bond surface bands are split by a gap of ≥ 0.27 eV throughout the zone. They show some dispersion of only about 0.2 eV. The Fermi level falls between the two bands, thus creating a semiconducting surface. To obtain a density-of-states curve for these bands a four-term Fourier expansion for the band energy $E(\vec{k}_{\parallel})$ has been fitted to the calculated band structure at the four $\vec{k}_{\parallel}$ points Γ, M', $\bar{M}$, and K', and subsequently evaluated over a fine grid of $\vec{k}_{\parallel}$ points of the two-dimensional Brillouin zone. The results are shown in Fig. 12 (bottom). Two structures are found separated by about 0.4 eV, corresponding to the two surface bands. The lower surface band, which overlaps with states arising from bulk and other surface bands, is centered at about $E = E_v = 0$. Experimental photoemission data[2,3] show structure at somewhat lower energy ($E \approx -0.5$ eV). Further lowering of the calculate surface band, and better agreement
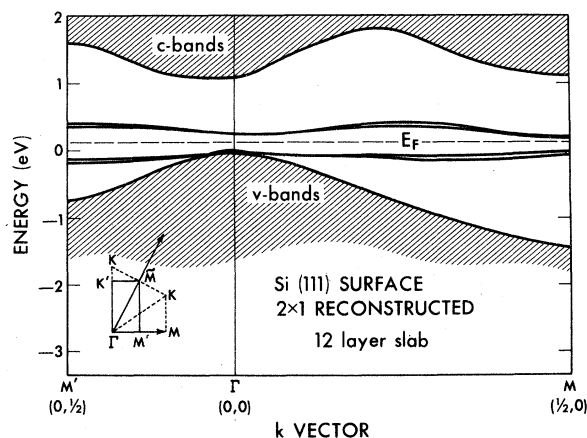
FIG. 11. Two-dimensional band structure around the fundamental gap for a (2×1) reconstructed Si(111) 12-layer film. Folded-back Brillouin zone is indicated in the insert.

with experiment, can probably be obtained by using a different choice of atomic displacement parameters. Our results, however, show the definite trend of splitting the dangling-bond surface bands combined with an over-all lowering because of the buckling structure.

Also indicated in Fig. 12 (top) is a joint density of states (JDS) for optical transitions between the lower and the upper surface bands. Matrix-element effects have not been considered in this plot. The
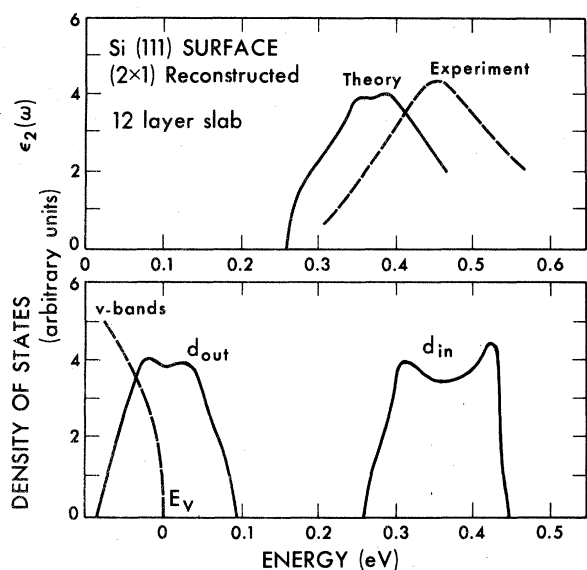

FIG. 12. Calculated joint density-of-states curve for low-energy transitions between dangling-bond bands of (2×1) Si(111) (top). Also indicated is the experimental absorption $\epsilon_2(\omega)$ as obtained in Ref. 4. Bottom figure shows the regular density of states for the two dangling-bond bands (d_{in} and d_{out}) of (2×1) Si(111).
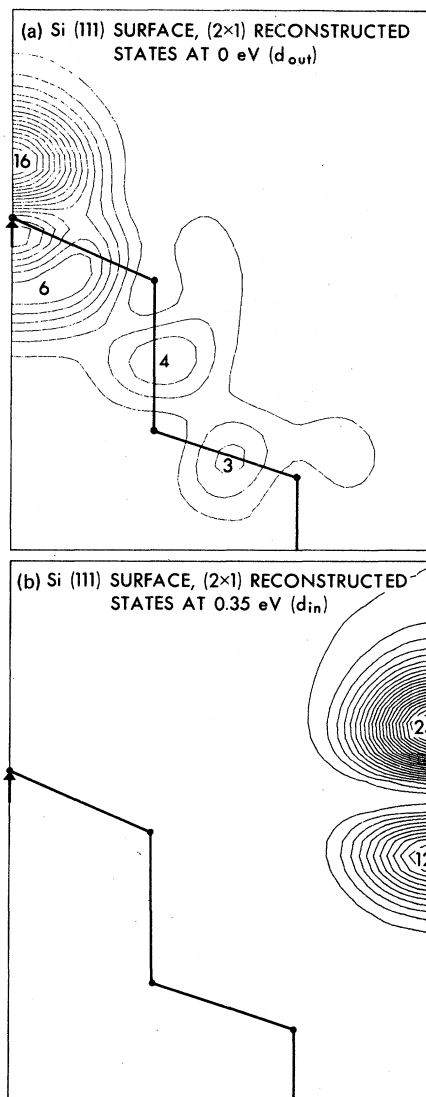

FIG. 13. Charge-density contour plots for the dangling-bond states d_{out} (top) and d_{in} (bottom) of (2×1) Si(111). Charge is plotted in a (210) plane of (2×1) Si which corresponds to the (110) plane of (1×1) Si. The raised and lowered atoms are marked by arrows.

JDS curve can be qualitatively compared to infra-red-absorption measurements[4] (broken line). A quantiative comparison is not reasonable because of the ad hoc choice of atomic displacement parameters, and because of probable strong excitonic effects. It is also instructive to calculate the charge-density distributions for states inside the two peaks in the density of states of Fig. 12 (bottom). The corresponding charge (or hypothetical charge for the unoccupied upper band) is displayed in Fig. 13 in a (210) plane intersecting the surface at right angle. This plane corresponds to the (110) plane of the unreconstructed surface. The buckling raises the

surface atom on the left-hand side and lowers the surface atom on the right-hand side. Owing to lateral shifts, the second-layer atoms are slightly moved out of the (210) plane. The states show very interesting real space behavior. Electrons in states originating from the lower peak labeled d_{out} are located predominantly on those atoms which have been raised and avoid those atoms which have been lowered. Conversely, the wave functions for unoccupied states of the peak labeled d_{in} are concentrated around those atoms which have been lowered. The surface thus exhibits a (2×1) pattern of nearly twofold occupied dangling-bond states centered at every second row of atoms. Roughly speaking, the unpaired dangling electron of every second-surface atom (in) is transferred to its neighboring atom (out) where it pairs up with another electron, thus creating an ionic semiconducting surface. In view of this picture infrared transitions are expected to have a very weak oscillator strength because of the small wave-function overlap. In fact, the calculated dipole matrix elements are of the order of $0.05 \times 2\pi/a_0$ and about one order of magnitude smaller than average bulk matrix elements. However, the net charge transfer obtained in our calculation is presumably too large and would be decreased by correlation effects. These effects can be considerable for bands of 0.3 eV width; since they are not included in our calculations, the results are of a more qualitative nature. It can be seen from Fig. 13 that the charge distribution of the lower peak (d_{out}) extends somewhat into the back bonds. This mixing of states happens around the Γ point where the lower dangling-bond band actually overlaps with lower-lying back-bond states. In fact, some of the transverse back-bond states (Γ_{tb}) found at -1.5 eV for the unreconstructed surface rise in energy upon reconstructed and fall between 0 and -0.8 eV. At $\tilde{k}_{\parallel}$ points further away from the Γ point $(K', M', \tilde{M})$ the dangling-bond surface bands have very pure dangling-bond character and do not show any noticeable mixing with the back bonds which decrease in energy to about -3.5 eV. The existence of transverse back-bonding surface states (or strong surface resonances) close to the valence-band maximum may explain angular photoemission results[9] involving states between 0 and -1.4 eV. These results show a threefold rotational pattern, as do the transverse back bonding states, but the pure longitudinal dangling-bond states do not. The results we obtained for the (2×1) reconstructed surface can be understood on the basis of simple chemical arguments. Since our calculations were based on Haneman's model, which excludes *bond length* variations (such as AH propose in their model), the various changes in the electronic structure must, in first order, be caused by *bond angle* variations. This concept is not new; in fact, Haneman's

original model was designed on this basis.

The following discussion includes three different bonds and their respective energies, i.e., the energies of a state whose changes are primarily concentrated in one of these bonds: the (longitudinal) dangling bonds d with energy ϵ_d, the transverse back bonds $b_t(\epsilon_t)$ between first and second atomic layer, and the longitudinal back bonds $b_l(\epsilon_l)$ between second and third atomic layer.

Let us consider the case of the *raised* outermost atom. In this case, the bond angles between the longitudinal orbitals and the transverse orbitals are increased whereas the bond angles among the transverse orbitals are decreased. The ideal sp^3 hybridization is consequently changed in such a way as to increase the amount of s-like character in the longitudinal orbitals and of p-like character in the transverse orbitals. As a consequence, the energy ϵ_d of the dangling bonds d is lowered owing to an increased s admixture. The transverse back bonds b_t now contain more p character which raises their energy ϵ_t and weakens the bonds. The longitudinal back bonds, like the dangling bonds, contain more s character which lowers their energy ϵ_l and strengthens them. The inclusion of bond-length variations (AH model) would result in an additional stretching of the transverse back bonds b_t and a further weakening. In the case of the *lowered* outermost atom, the bond angles change the opposite way causing a decrease of s character in the longitudinal orbitals and an increase of p character in the transverse orbitals. The energy ϵ_d of the dangling bonds d is raised, the energy ϵ_t of the transverse back bonds b_t is lowered, combined with a strengthening of the bonds (an additional bond-length contraction would increase this effect), and the energy ϵ_l of the longitudinal back bonds b_l is increased, combined with a weakening of the bonds. Raising and lowering of alternating rows of atoms leads in first order to a combination of the above effects. The net effect on the longitudinal back bonds cannot be anticipated in this simple picture. The simple picture apparently underlies our self-consistent pseudopotential results. It accounts for the following facts: (a) The strengthening of the transverse back bonds and the weakening of the longitudinal back bonds in the relaxed (1×1) geometry (here the transverse back bonds have also been contracted); (b) the raising of the dangling-bond energy ϵ_b at Γ in the relaxed (1×1) geometry; (c) the more s-like character of the lower dangling-bond band in the (2×1) geometry as compared to the upper more p_z-like dangling-bond band [this can be recognized from the dangling-bond charge having a different asymmetry around the outermost atoms in Fig. 13 (top and bottom)]; (d) the localization of the lower occupied dangling-bond orbitals on the raised atoms and of the higher unoccupied dangling-bond

orbitals on the lowered atoms in the (2×1) geometry; and (e) the raising of the transverse back-bond energies ϵ_t up to about -0.5 eV at Γ and -3.5 eV at K' for back bonds connected to raised outermost atoms in the (2×1) geometry.

V. CONCLUSIONS

A recently developed extension[19] of the empirical pseudopotential method for the self-consistent treatment of local "nonperiodic" configurations has been applied to several Si (111) surface models. Three different surface models have been studied including unreconstructed, relaxed, and unrelaxed (1×1) surfaces which also have been investigated by Appelbaum and Hamann[10] in the only previously existing self-consistent calculation. Their results are basically consistent with our calculations. In addition, new types of surface states corresponding to the longitudinal back bonds between the second and third atomic layer are found, and complete density of states curves are presented. A buckled (2×1) surface model such as proposed by Haneman (with preserved back bond lengths) has been used to study the (2×1) reconstructed surface. The salient experimental results on (2×1) Si (111) surfaces can be understood on the basis of this model. Upon reconstruction, the dangling-bond band is split and

lowered considerably in energy. The surface is found to be semiconducting producing an infrared absorption peak at low energies. Transverse back-bonding surface states are found to be raised in energy and appear between 0 and -0.5 eV below the valence-band edge at Γ and above -3.5 eV at K'. These states may be the origin of the angular-dependent photoemission results.

The various effects are discussed on chemical grounds in terms of bond angle variations occurring with reconstruction. Changes in back-bond lengths, such as claimed by AH in a recent paper[31] to be *essential*, are thus *not necessary* for a satisfactory explanation of spectroscopic data. The existence of bond-length changes, however, cannot be ruled out on the basis of the existing results since both bond-angle and bond-length variations seem to alter the electronic structure at the surface in a similar manner.

ACKNOWLEDGMENTS

*Supported in part by the National Science Foundation Grant No. DMR72-03206-AO2.

†Swiss National Science Foundation fellow.

‡National Science Foundation graduate fellow.

[1]Experimental literature through 1973 is compiled by W. Mönch, in *Festkörperprobleme*, edited by J. H. Queisser (Pergamon, New York, 1973), Vol. XIII, p. 24.

[2]D. E. Eastman and W. D. Grobman, Phys. Rev. Lett. 28, 1378 (1972).

[2]L. F. Wagner and W. E. Spicer, Phys. Rev. Lett. 28, 1381 (1972).

[4]G. Chiarotti, S. Nannarone, R. Pastore, and P. Chiaradia, Phys. Rev. B 4, 3398 (1971).

[5]J. E. Rowe and H. Ibach, Phys. Rev. Lett. 31, 102 (1973).

[6]J. E. Rowe and H. Ibach, Phys. Rev. Lett. 32, 421 (1974).

[7]H. Ibach and J. E. Rowe, Surf. Sci. 43, 481 (1974).

[8]J. E. Rowe and J. C. Phillips, Phys. Rev. Lett. 32, 1315 (1974).

[9]J. E. Rowe, M. M. Traum, and N. V. Smith, Phys. Rev. Lett. 33, 1333 (1974).

[10]J. A. Appelbaum and D. R. Hamann, Phys. Rev. Lett. 31, 106 (1973), Phys. Rev. Lett. 32, 225 (1974); and Phys. Rev. B 8, 1777 (1973).

[11]S. Ciraci and I. P. Batra, Solid State Commun. 16, 1375 (1975).

[12]K. C. Pandey and J. C. Phillips, Phys. Rev. Lett. 32, 1433 (1974).

[13]M. Schlüter, J. R. Chelikowsky, S. G. Louie, and M. L. Cohen, Phys. Rev. Lett. 34, 1385 (1975); and M. Schlüter, J. R. Chelikowsky, and M. L. Cohen, Phys. Lett. A 53, 217 (1975).

[14]J. A. Appelbaum and D. R. Hamann, Phys. Rev. B 6, 2166 (1972).

[15]G. P. Alldredge and L. Kleinman, Phys. Rev. Lett. 28, 1264 (1972).

[16]G. P. Alldredge and L. Kleinman, Phys. Rev. B 10, 559 (1974).

[17]M. L. Cohen and V. Heine, in *Solid State Physics*, edited by H. Ehrenreich, F. Seitz, and D. Turnbull (Academic, New York, 1970), Vol. 24, p. 37.

[18]E. Mooser, M. Schlüter, and I. Ch. Schlüter, J. Phys. Chem. Solids 35, 1269 (1974).

[19]M. L. Cohen, M. Schlüter, J. R. Chelikowsky, and S. G. Louie, Phys. Rev. B (to be published).

[20]G. Gilat and G. Dolling, Phys. Lett. 8, 304 (1964).

[21]J. C. Slater, Phys. Rev. 81, 385 (1951); W. Kohn and L. J. Sham, *ibid.* 140, A1133 (1965).

[22]E. P. Wigner, Phys. Rev. 46, 1002 (1934).

[23]I. V. Abarenkov and V. Heine, Philos. Mag. 12, 529 (1965).

[24]J. R. Chelikowsky and M. L. Cohen, Phys. Rev. B 10, 5095 (1974).

[25]J. P. Walter and M. L. Cohen, Phys. Rev. B 4, 1877 (1971).

[26]N. D. Lang and W. Kohn, Phys. Rev. B 1, 4555 (1970).

[27]L. Falicov and F. Yndurain, J. Phys. C 8, 147 (1975); and 8, 1563 (1975).

[28]J. D. Joannopoulos and M. L. Cohen, Phys. Rev. B 7, 2644 (1973).

[29]D. Haneman, Phys. Rev. 121, 1093 (1961).

[30]A. Taloni and D. Haneman, Surf. Sci. 10, 215 (1968).

[31]J. A. Appelbaum and D. Hamann, Phys. Rev. B 12, 1410 (1975).